

Article

A Case Study and Numerical Modeling of Post-Wildfire Debris Flows in Montecito, California

Diwakar K. C. [†], Mohammad Wasif Naqvi [‡] and Liangbo Hu ^{*}

Department of Civil and Environmental Engineering, University of Toledo, Toledo, OH 43614, USA; diwakar.kc@rockets.utoledo.edu (D.K.C.); naqvimo1@msu.edu (M.W.N.)

* Correspondence: liangbo.hu@utoledo.edu

[†] Current address: Geotechnology LLC, 1780 Carillon Blvd, Cincinnati, OH 45240, USA.

[‡] Current address: Department of Civil and Environmental Engineering, Michigan State University, East Lansing, MI 48824, USA.

Abstract: Wildfires and their long-term impacts on the environment have become a major concern in the last few decades, in which climate change and enhanced anthropogenic activities have gradually led to increasingly frequent events of such hazards or disasters. Geological materials appear to become more vulnerable to hazards including erosion, floods, landslides and debris flows. In the present study, the well-known 2017 wildfire and subsequent 2018 debris flows in the Montecito area of California are examined. It is found that the post-wildfire debris flows were initiated from erosion and entrainment processes and triggered by intense rainfall. The significant debris deposition in four major creeks in this area is investigated. Numerical modeling of the post-wildfire debris flows is performed by employing a multi-phase mass flow model to simulate the growth in the debris flows and eventual debris deposition. The debris-flow-affected areas estimated from the numerical simulations fairly represent those observed in the field. Overall, the simulated debris deposits are within 7% error of those estimated based on field observations. A similar simulation of the pre-wildfire scenario indicates that the debris would be much less significant. The present study shows that proper numerical simulations can be a promising tool for estimating post-wildfire erosion and the debris-affected areas for hazard assessment and mitigation.



Citation: K. C., D.; Naqvi, M.W.; Hu, L. A Case Study and Numerical Modeling of Post-Wildfire Debris Flows in Montecito, California. *Water* **2024**, *16*, 1285. <https://doi.org/10.3390/w16091285>

Academic Editor: Weijie Zhang

Received: 15 March 2024

Revised: 17 April 2024

Accepted: 24 April 2024

Published: 30 April 2024



Copyright: © 2024 by the authors. Licensee MDPI, Basel, Switzerland. This article is an open access article distributed under the terms and conditions of the Creative Commons Attribution (CC BY) license (<https://creativecommons.org/licenses/by/4.0/>).

1. Introduction

Widespread wildfires around the world are occurring every year at an alarmingly increasing frequency, which may be aggravated by climate change and enhanced human activities [1–4]. Wildfires can have significant impacts on the environment, climate and ecosystems. They may also cause considerable alterations in geological materials that appear to become more vulnerable to various gravity-driven mass movements such as landslides, debris flows and mudslides. Post-wildfire incidents including overland flow, excessive erosion and debris flows have been widely reported [5–7]. It has been speculated that post wildfire, soils or sediments may become more resistant to water infiltration while more susceptible to erosion [8–10], thus leading to an increased overland flow (or surface runoff), enhanced soil erosion, and favorable conditions for debris flows after intensive rainfall. There has been growing interest in the investigation of post-wildfire debris flow processes, e.g., their initiation, triggering conditions, sediment entrainment and flow characteristics. Meyer et al. [11] studied the post-fire debris flow in Yellowstone National Park and concluded that it grew by runoff bulking of the eroded sediment from the channel and hillslope, and there was no major contribution from landslides or slope failures in the generation of debris materials. Cannon and Reneau [12] found extensive erosion of the soil in the hillslopes during the summer thunderstorms after the 1996 Dome fire in the Capulin Canyon in New Mexico, which resulted in at least one debris flow. From a field survey of 46 post-wildfire debris flows in Utah, Colorado

and South California, Santi et al. [5] reported significant bulking of debris flows by erosion and scour rather than from landslides and slope failures. Kean et al. [13] investigated the post wildfire debris flows in San Gabriel and Santa Ynez Mountains in California and found that the debris flows were initiated primarily by surface-water-runoff-related processes. Cannon et al. [14] also showed that wildfire-related debris flow at Storm King Mountain, Colorado, was mainly initiated by eroded hillslope materials and progressive entrainment by overland flows. Nyman et al. [15] reported that the erosion initiated post-fire debris flows in a dry eucalyptus forest in southeastern Australia. These studies suggest that it is crucial to consider the enhanced overland flow and the erosion of hillslope and channel materials as major factors in simulations of the initiation and growth of post-fire debris flows.

The present study is aimed to numerically examine the case of debris flows in Montecito (California) with the main focus on the effects of the wildfire in this area. The behavior of a debris flow in motion is very complex and involves potentially strong interactions among different material phases. Theoretical efforts to better understand the behavior of granular flows can be traced to Bagnold [16], Savage [17] and Takahashi [18]. Most of the models developed earlier are single-phase models which generally consider the flow as a Newtonian, Bingham or dilatant fluid [19–21]. Granular frictional flow models were proposed for coarse-grained dry mass flows [22–25], while the visco-plastic model for dense granular flows was proposed by Jop et al. [26]. A number of models adopted a mixture approach [27–31] in an effort to address the overall complex behavior of the material and model its evolution as a solid/fluid mixture. Overall, the core challenge in model development is the proper representation of the distinctive behavior of debris material that contains various constituents such as water, colloidal solids, fine particles and larger particles like cobbles and boulders. The present study explores a multi-phase flow model recently developed by Pudasaini and Mergili [32] that considers multiple phases in motion and incorporates many essential physical aspects of debris flows. It considers three phases in the debris flow: coarse particles like boulders, cobbles and gravel as the solid phase; fine particles including fine gravel and sand as the fine-solid phase; and fluid (water combined with silt and clay) as the fluid phase. This model is also capable of considering the soil erosion or entrainment joining the flowing debris. In the present study, the post-wildfire debris flows that took place in Montecito, California, on 9 January 2018 are surveyed and subsequently investigated numerically using this multi-phase modeling tool.

2. Study Area

The present study is focused on the 2018 Montecito debris flows, which took place in the vicinity of Montecito Peak in Santa Barbara County, California, as shown in Figure 1. In the north of the study area are the Santa Ynez Mountains, whose rock formations are predominantly made of weak sandstones and shale and are susceptible to weathering and incision [33]. There are considerably loose soil layers on the rock surface of these mountains due to excessive weathering. Oriented east–west in the study area, human settlements are well established from the foot of these mountains to the coastline of the Pacific Ocean. Several small channels flow dendritically, forming four major creeks that travel through the human settlements, i.e., Montecito Creek, San Ysidro Creek, Buena Vista Creek and Romero Creek. The temperature in this area ranges from approximately 6 °C in December and January to around 27 °C in September. The average annual rainfall in this area is approximately 486 mm; typically, the driest month is July, with around 0.5 mm of rainfall, and the wettest is February, with around 113 mm of rainfall. Nonetheless, across this area, substantial variations and extreme rainfall events are common [34,35].

The area significantly affected by constant wildfires is in the Santa Ynez Mountain range. Figure 2 shows the slope map of this region; the slope of most of the mountains is greater than 30°, but the area in the southern part of the mountains with considerable human settlements is less steep. The highest elevations of the catchment area for Montecito Creek, San Ysidro Creek, Buena Vista Creek and Romero Creek are 962.0 m, 967.8 m, 512.1 m

and 895.6 m, respectively, while their catchment areas are 12.48 km^2 , 7.84 km^2 , 1.74 km^2 and 5.15 km^2 , respectively.

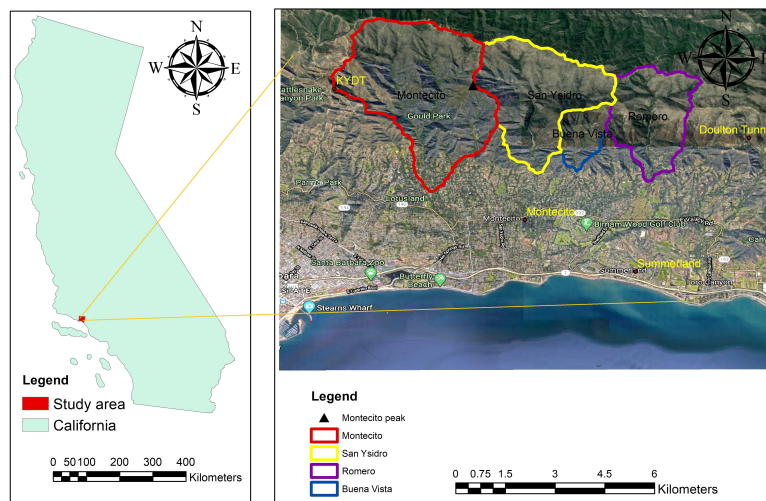


Figure 1. The study area located at Montecito peak in California.

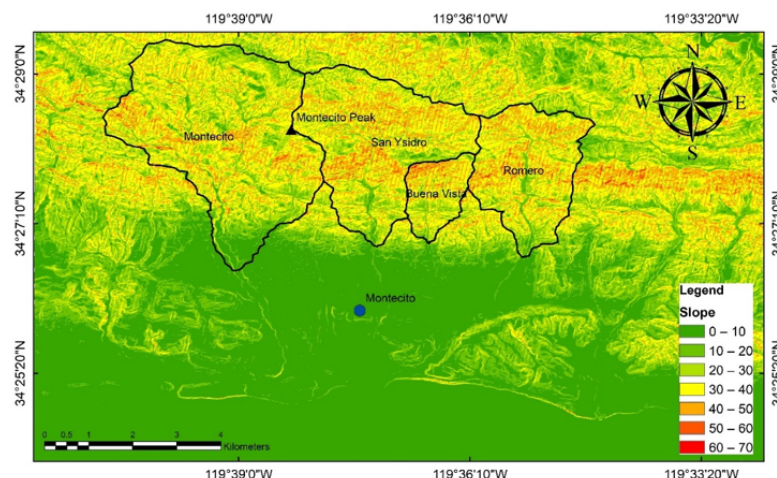


Figure 2. Slope map of the study area, including the catchment area of the four major creeks highlighted; the blue dot indicates the town of Montecito.

3. Background on 2018 Debris Flows

3.1. Wildfire and Burnt Areas

The present study is focused on the post-wildfire geological hazards after a massive wildfire, which was later named the Thomas fire, broke out from a line slab at Thomas Aquinas College on 4 December 2017. It burnt approximately 1140 km^2 , including many parts of the San Ynez Mountains in the northern part of Montecito. A total of 1063 structures were destroyed and two casualties were reported [36]. The wildfire was finally fully contained after forty days.

In the present study, remote-sensing-based data available from various agencies worldwide were used to identify the wildfire-affected areas. The present study utilized two major data sources: the Landsat satellite images produced by the National Aeronautics and Space Administration (NASA) [37], and the Sentinel satellite images captured by the European Space Agency (ESA) that are available from the Copernicus Open Access Hub [38].

It is of interest to examine the Landsat 8 data from 25 December 2017 after the fire [37] to identify the areas most affected by the Thomas fire. Different RGB false color

maps [39–41] can be processed to determine the fire-affected areas based on the light absorption and reflection of the plants. Vegetation and plant pigments typically absorb red and blue lights while reflecting green light. Therefore, the areas that are able to retain most of their vegetation appear green, as green light is reflected while the red and the blue lights are absorbed by plants. Meanwhile, the wildfire-burnt areas appear reddish after the plants have been burned. Indeed, Figure 3 presents the burnt areas that appear reddish in the entire study area. The yellow square in Figure 3 indicates the area with post-wildfire debris flows that is the focus of the subsequent numerical investigation.

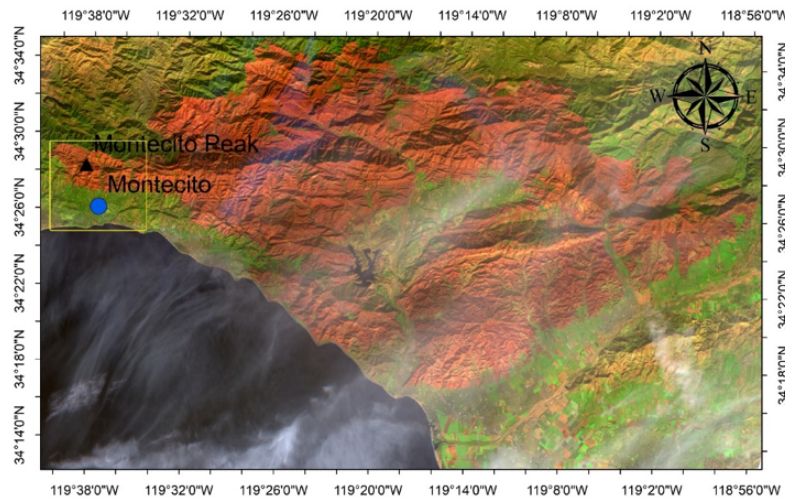


Figure 3. The RGB image of the region showing the area burnt by the Thomas wildfire; the blue dot indicates the town of Montecito.

3.2. Relevant Rainfall Records before and during the Debris Flows

It is of great interest to examine the rainfall data before and during the studied debris flows in the present study. Table 1 summarizes the total rainfall on 8 January and 9 January 2018, recorded by the National Oceanic and Atmospheric Administration [35] at several rain gauge stations around the study area. Figure 4 shows the elevation of this region, where the rainfall stations are also marked. It is of particular relevance to examine the rainfall around the time of the debris flow event. The three-hour interval data from Santa Barbara station (Figure 4) were available from an online database maintained by Zoomash Ltd., UK [42]. Figure 5 shows the cumulative rainfall with time in hours starting at 12:00 a.m. on 7 January 2018, along with the same date for the year of 2017 for a comparison. It is worth noting that the total rainfall between these two periods of 2017 and 2018 is almost the same; the cumulative rainfall in the 96 hr period (from 12 a.m. on 7 January 2017 to 9 p.m. on 10 January 2017) is 47.7 mm, while the cumulative rainfall for the same period (from 12 a.m. on 7 January 2018 to 9 p.m. on 10 January 2018) is 47.4 mm. However, it is evident that in 2018, the rain intensified enormously around 9 January, which coincides with the initiation of the debris flows.

Although at the Santa Barbara station, the cumulative rainfall at these two years is comparable, there are substantial variations in rainfall along with extremely high intensities throughout the study area [34,35]. Table 1 clearly reveals the significant difference in the spatial distribution of rainfall around the study area. These results suggest that the rainfall was clearly greater in the mountains (KYDT, Edition Trail, Doulton Tunnel) than in the lower lands along the coast (Summerland, Montecito, CA, USA) of the region. It is possible to speculate that the high-intensity rainfall that occurred in the steep mountain slopes was likely the trigger for the subsequent debris flows. Table 1 also summarizes the maximum one-hour rainfall in these rainfall stations recorded by NOAA. It can be observed that almost half of the 24-h rainfall occurred in one hour. Although there was some modest rainfall on 8 January 2018, no debris flows were observed until the above-mentioned high-

intensity rainfall storm [34]. Therefore, in this study, the 1 hr high-intensity rainfall around the catchments is considered in further analyses.

Table 1. Rainfall data recorded at different rain gauge stations, including the total rainfall during the two-day period of 8 January and 9 January 2018, and the peak one-hour rainfall recorded by NOAA on 9 January 2018 [35].

Station ID	Station	Elevation (m)	Total Rainfall (mm)	Peak Rainfall (mm)
227	KTYD	724	81	28
231	Doulton Tunnel	541	91	39
252	Edison Trail	503	80	37
325	Montecito	41	54	24
328	Summerland	26	56	26
208	Carpinteria Fire	9	61	35

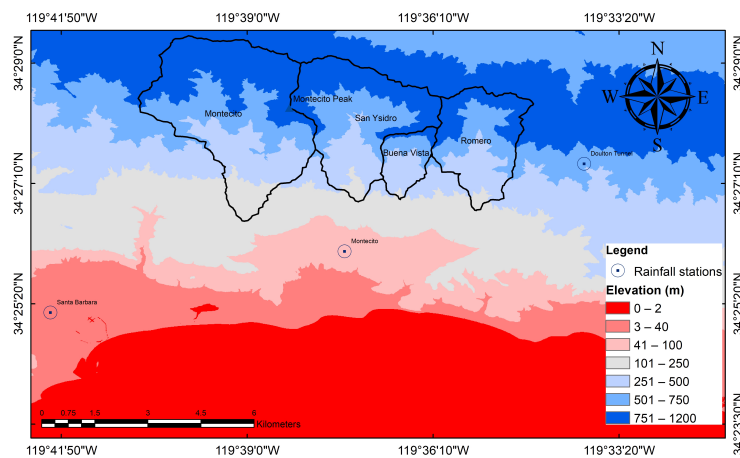


Figure 4. The locations of different rainfall stations in the elevation map.

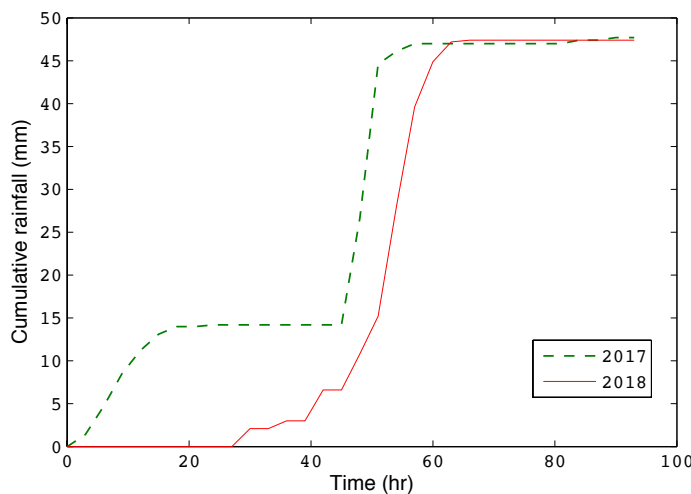


Figure 5. Cumulative rainfall starting at 12 a.m. on 7 January in 2017 and 2018 at Santa Barbara station.

3.3. Field Observations of the Debris Flows

The sediment in the debris flow originated from the hillslopes. However, the surface of the steep mountains in this area was highly eroded after the rainfall, likely contributing to the growth in the debris flows. Both rill and inter-rill erosion was observed in the watershed, but no evidence of major landslides was found. The deposited materials contained viscous

fluid produced by the mixture of fine soil and water. Large boulders were deposited in the depositional basin, which were subsequently transported from the upstream to the downstream along with the concentrated flow. Some bank erosion resulting from the large upstream flow also supplied boulders to the flow. For example, one of the primary sources for the debris material was identified to be the erosion of the watershed in the Santa Ynez Mountains [34,43,44]. Kean et al. [34] also reported considerable rill and inter-rill erosion in the basins, as the burned hillslopes with numerous rills in the Santa Ynez mountains supplied materials for the debris flows after the rainfall. Hence, it is concluded that the bulk of the debris flow resulted from significant erosion.

All of the four major creeks experienced massive debris flows, which led to substantial destruction around the creeks. The destruction was extremely devastating around Montecito Creek and San Ysidro Creek. The debris-flow-affected areas can be clearly observed in the satellite images. Each of the images in Figures 6–8 obtained from the Google Earth shows both the image captured in April 2017 before the debris flow and the image in April 2018 after the debris flow at the same location.

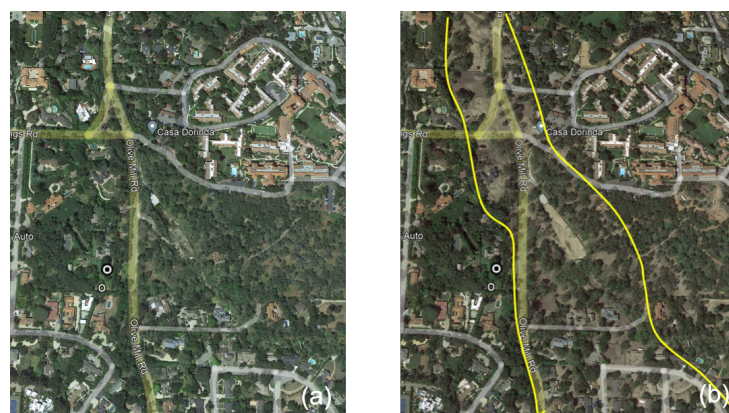


Figure 6. Area around Montecito Creek (a) before and (b) after debris flows; the area between the yellow lines highlights the main area affected by the debris flows.

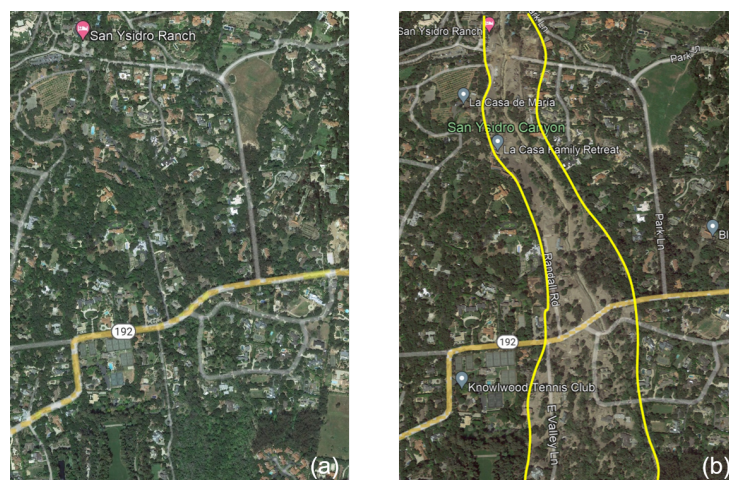


Figure 7. Area around the San Ysidro Creek (a) before and (b) after debris flows around Highway 192 in Montecito; the area between the yellow lines highlights the main area affected by the debris flows.

Figure 6 shows the debris-flow-affected area around Olive Mill Road. In Figure 6a, there are more green areas including those under the trees covered by grass. In Figure 6b, there are much less green areas under the trees, as the deposited debris flow covered the vegetation under the trees. Figure 7a shows the area around the San Ysidro Creek before the debris flow, while Figure 7b clearly shows the debris flow channel along the downstream of San Ysidro Ranch; the areas affected around Highway 192 are also clearly visible. The

area around Romero Creek before and after the debris flows is shown in Figure 8. The differences are particularly evident inside the red circles highlighted in the figure.



Figure 8. Area around Romero Canyon Road (a) before and (b) after the debris flow in Romero Creek; the area circled by the red line indicates the main area affected by the debris flows.

Table 2 summarizes the debris volumes in the four major creeks estimated from field observations by Kean et al. [34]; close to $230,000 \text{ m}^3$ of debris was deposited around Montecito Creek and over $300,000 \text{ m}^3$ was deposited around San Ysidro Creek, while the deposition around Romero Creek and Buena Vista Creek is far more modest. These estimations are assessed in the numerical simulations presented in the following section.

Table 2. The observed debris volume in different creeks (source: Kean et al. [34]).

Creek	Observed (m^3)
Montecito	231,000
San Ysidro	297,000
Buena Vista	41,000
Romero	100,000

4. Numerical Modeling

4.1. Background

In the present study, the debris flows are simulated based on a recently developed multi-phase model [32] that considers three phases of debris material in motion and incorporates many essential physical aspects of mass flows. It expands the theoretical formulations of a two-phase, i.e., solid and fluid, model of Pudasaini [30] with the introduction of a fine-solid phase; this allows more complex material behavior to be addressed in the modeling of the flow process. The first phase, termed as the fluid phase, is considered to be a mixture of water and very fine particles such as silt, clay and colloids. The fluid rheology is considered to be shear-rate-dependent Herschel–Bulkley viscoplastic. The second phase, termed as a fine solid, contains fine gravel and sand. Its rheology is characterized by rate-dependent visco-plastic behavior [26]. The constitutive behavior of this phase is modeled as shear- and pressure-dependent Coulomb viscoplasticity; both viscous stress and yield stress can considerably affect the behavior of fine solids. The third phase, termed the solid phase, consists of coarse particles including boulders, cobbles and gravel. Such particles are generally believed to behave like a frictional material, for which the Mohr–Coulomb

plasticity model can be used. This multi-phase model has been employed for large-scale simulations of real-world events and has shown promising potential [45–48].

This model is implemented in an open-source computational package, r.avaflow 2.1 [46]. It supports GIS-based applications for numerical simulations on available actual topographies. It is freely available as a raster module of GRASS GIS 8.3 software, employing the programming languages Python and C along with the statistical software R 4.2 [46]. It is noted that this model is able to include the erosion or entrainment of sediment along the path of the flow; the erosion is considered as a function of kinetic energy and characterized by an erosion coefficient.

The details of the relevant mathematical formulations can be found in Pudasaini [30] and Pudasaini and Mergili [32]. Digital elevation model (DEM) data of the study area are required to run the simulations on the actual topography. The 12.5 m high-resolution terrain-corrected DEM data were retrieved from the Alaska Satellite Facility [49]. The background images were obtained from Google Earth and were georeferenced using GIS when they were used in the simulations.

4.2. Field-Scale Simulations of Post-Wildfire Debris Flows

In the present simulations, the 30 mm of rainfall over 1 hr is considered to be the trigger for the debris flows, based on the rainfall data recorded in the three stations around the catchments, i.e., Doulton Tunnel, KYDT, and Montecito (Table 1). The average rainfall recorded in these three station is considered as the effective rainfall. Table 3 summarizes the key material parameters in the numerical simulations. The internal friction angle represents the internal frictional resistance for the solid or fine-solid phase, and the basal friction angle characterizes the frictional resistance of the bed material on which the mass flow moves, whereas for the fluid phase, such frictional resistances are considered to be 0. The erosion or entrainment that played a significant role in the growth in the debris flow, as discussed in Section 3.3, is thereby considered in the numerical simulation and characterized by an erosion coefficient.

Table 3. Input parameters for post-wildfire debris flow simulations. Note that s and fs represent the solid phase and fine solid phase, respectively.

Creek	Internal Angle (s , fs)	Basal Friction (s , fs)	Erosion Coefficient
Montecito	(25° , 10°)	(4° , 2°)	2.57×10^{-8}
San Ysidro	(25° , 10°)	(5° , 2°)	8.91×10^{-8}
Buena Vista	(25° , 10°)	(3° , 2°)	1.02×10^{-7}
Romero	(25° , 10°)	(8° , 4°)	7.94×10^{-8}

4.2.1. The Montecito Creek Debris Flows

The numerical simulation generates 215,500 m³ of debris, which is only 6.69% less than that observed in the field (Table 2). The final deposition, termed as the final change in basal topography by the output, is presented in Figure 9a, and the maximum flow height, also termed the flow depth, is shown in Figure 9b. The values in the figures represent the deposition depth or the flow velocity. The outermost contour represents the lowest value and the innermost the maximum value. Figure 9 also indicates the affected area, but the flow at its final stage is directed towards the east, while in the field, it was directed towards the west because the flow could not pass under Highway 101 due to the bridge [34]. Such human-made features are not part of the DEM and thus cannot be considered in this simulation. Overall, the simulation results reflect the observed debris-flow-affected area fairly well, and the simulated volume of debris material is reasonably close to the field estimation.

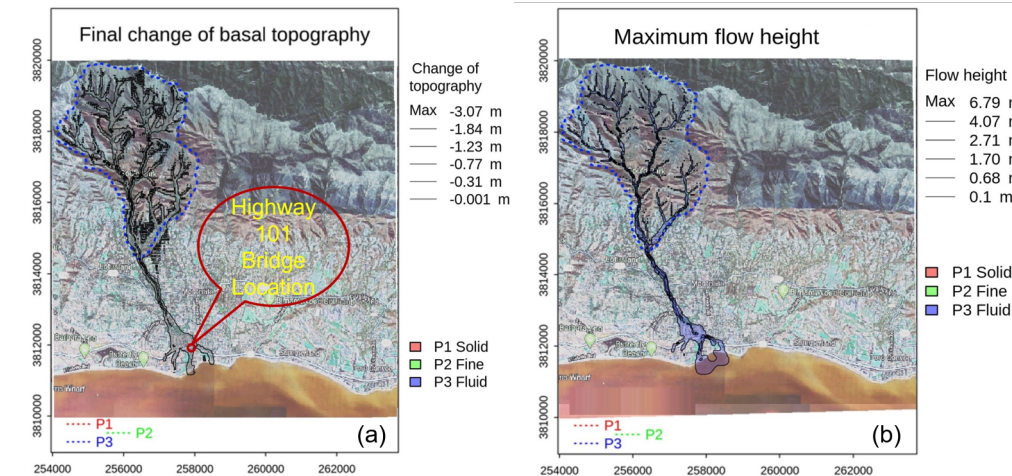


Figure 9. (a) Final deposition and (b) maximum flow height at Montecito Creek.

4.2.2. The San Ysidro Creek Debris Flows

A volume of 306,022 m³ of debris is generated by the numerical simulation, which is just 3% higher than the volume estimated in the field. The final deposition and runout distance are shown in Figure 10a. The maximum flow depth is shown in Figure 10b. Figure 10 shows that most of the deposition is close to the mountains. The flow-affected area shown in Figure 10 matches closely with the actual flow-affected area observed in the field as reported by Kean et al. [34]. The volume of debris generated is also very consistent with the estimated debris volume in the field (Table 2).

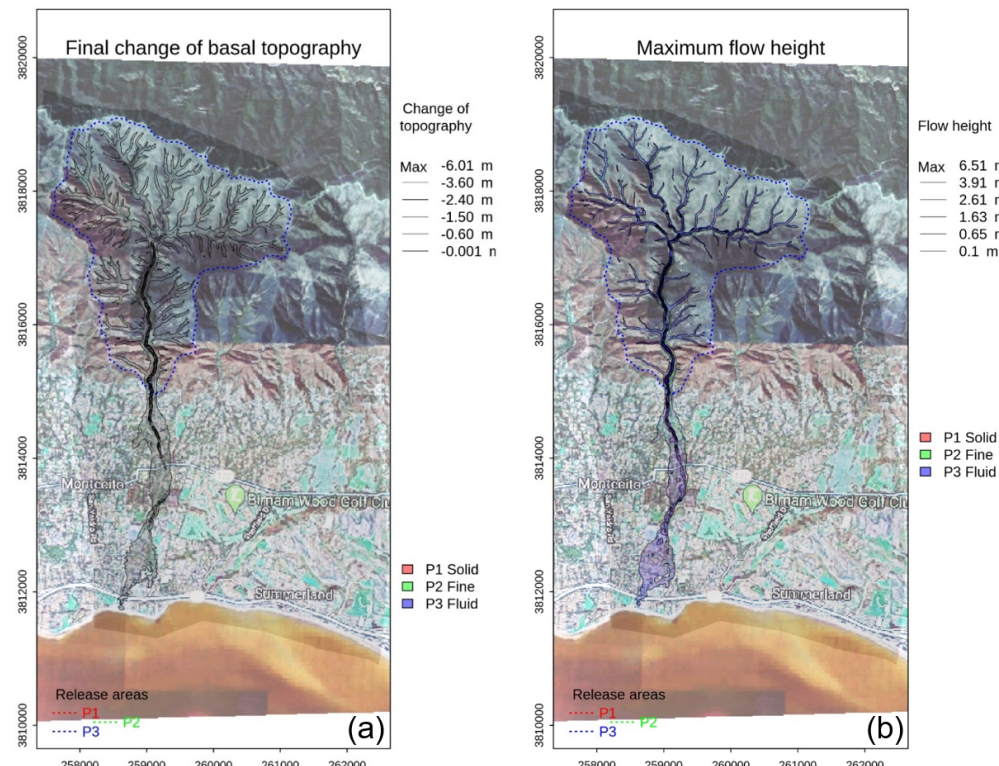


Figure 10. (a) Final deposition and (b) maximum flow height at San Ysidro Creek.

4.2.3. The Buena Vista Creek Debris Flows

The numerical simulation produces 39,320 m³ of debris, which is just 4% lower than the volume estimated in the field. The final deposition and the maximum flow depth are

given in Figure 11a,b, respectively. The simulated debris volume and affected areas are very close to the estimated debris volume and affected areas in the field [34].

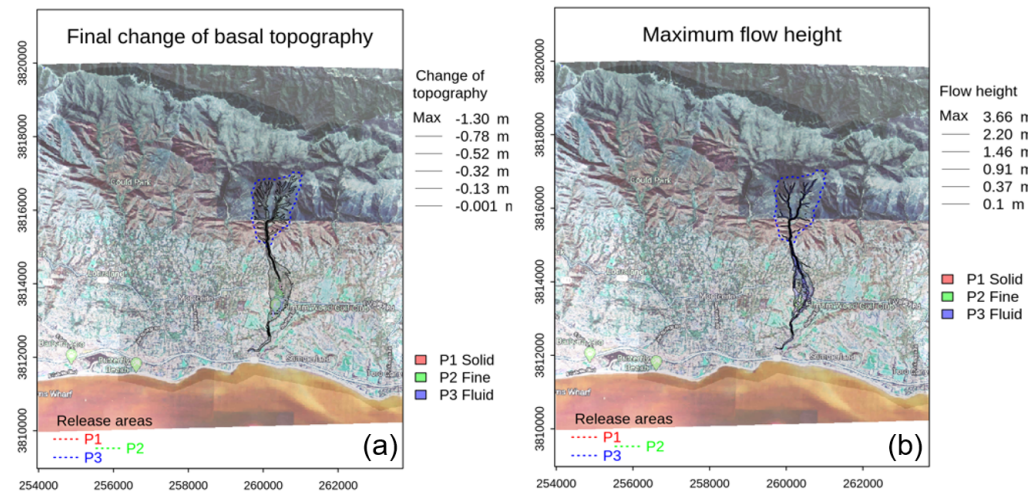


Figure 11. (a) Final deposition and (b) maximum flow height at Buena Vista Creek.

4.2.4. The Romero Creek Debris Flows

The simulated volume of 101,160 m³ of debris is 1.16% higher than the volume estimated in the field. The final change in basal topography and maximum flow height are given in Figure 12a,b, respectively. Figure 12 shows that the results fairly represent the affected areas.

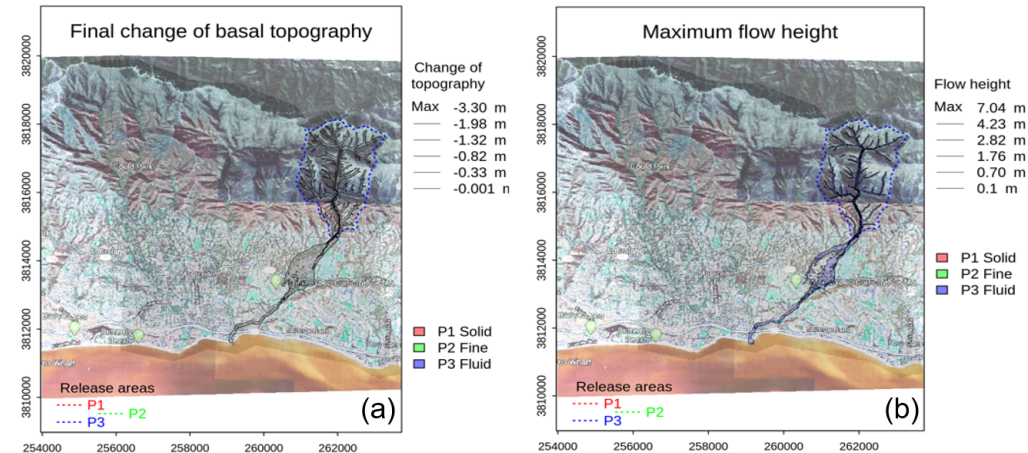


Figure 12. (a) Final deposition and (b) maximum flow height at Romero Creek.

Figure 13 presents the simulation of the debris across the four creeks. It is reasonably reflective of the pattern indicated from field observations [34]. Overall, the simulation results are consistent with the field estimations in terms of debris volume, runout distance and the area affected by the debris flow. Table 4 summarizes the simulated debris flow volumes as well as the estimated volumes based on the field observations reported by Kean et al. [34]. In Table 4, the debris volume in Montecito Creek exhibits the largest discrepancy with the estimated debris volume in the field in terms of percentage, but nonetheless, this is no more than 7%. Montecito Creek has the lowest erosion coefficient and Buena Vista Creek has the highest erosion coefficient, but the volumes of debris generated in both creeks are slightly underestimated. In terms of basal friction, Romero Creek has the highest basal friction, and for the other creeks, they are similar. For San Ysidro Creek, the debris volume generated is slightly higher than the debris volume estimated in the field, but the

debris-flow-affected area is lower than in the field, although the basal frictions applied are similar to other creeks.

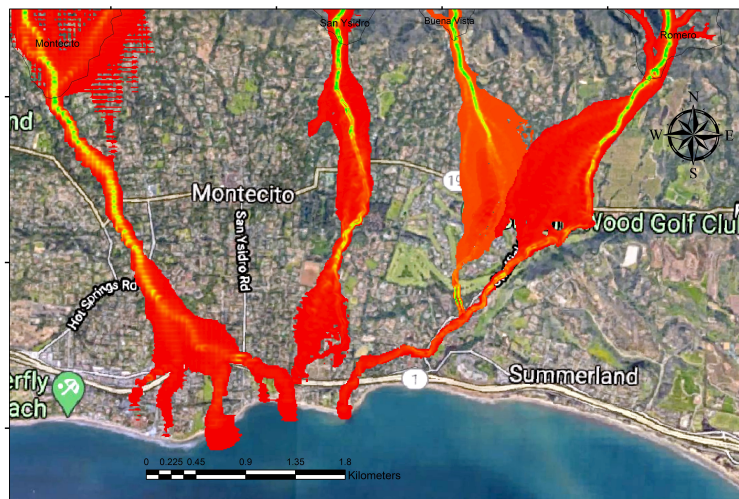


Figure 13. Simulation of debris-flow-affected areas; the areas highlighted in red indicate the debris-flow deposits.

Table 4. Summary of simulation results; note that the estimated volume is retrieved from Kean et al. [34] based on a field survey. Note that s and fs represent the solid phase and fine solid phase, respectively.

Creek	Estimated (m^3)	Simulated (m^3)	Difference (%)	Erosion Coefficient	Basal Friction (s, fs)
Montecito	231,000	215,500	−6.69	2.57×10^{-8}	(4°, 2°)
San Ysidro	297,000	306,022	+3.04	8.91×10^{-8}	(5°, 2°)
Buena Vista	41,000	39,320	−4.10	1.02×10^{-7}	(3°, 2°)
Romero	100,000	101,160	+1.16	7.94×10^{-8}	(8°, 4°)

The difference in the erosion coefficient required for a proper estimation of debris volume can be attributed to several reasons. For instance, for all the simulations, 39 mm of rainfall over 1 h was applied; however, it is debatable that the rainfall might have varied considerably across the study area. There were no rainfall gauge stations within the catchments of these creeks in the Santa Ynez Mountain range, but a high spatial variation in rainfall intensity and rainfall amount was reported by NOAA during the debris flow event. Therefore, one of the main factors may be the differences in rainfall intensity and total rainfall at different locations. Another reason may be that in the simulation, each of the solid, fine solid and fluid phases is assigned a particular set of parameters, but the effects of the variations among soil types and properties from different locations are not addressed; in addition, the erosion is prescribed in the numerical model to be a function of the kinetic energy of the flow without further consideration of the soil erodibility. In a numerical simulation of debris flows initiated from erosion without any wildfire effects, Baggio et al. [50] reported the debris volume generated within a error of 20% using the same model as in the present study; the results obtained from the present study are within a 6.69% error and can be possibly considered as fairly reasonable.

4.3. Simulations of Pre-Wildfire Debris Flows

It is of interest to explore a hypothetical scenario of debris flows before the wildfire for the sake of comparison. In this section, simulations of possible flows in the four major creeks

under pre-wildfire conditions are conducted. Compared to the post-wildfire scenarios, the surface roughness in the pre-wildfire scenario may be considerably higher [51]; therefore, the basal friction is increased in this section. The infiltration capacity of soil is also reduced after a wildfire [9,10]; therefore, the effective rainfall that evolved into overland flow is considered to be 18 mm in this section, decreased from the 30 mm in the post-wildfire debris flow simulations. Another significant change is the decreased erosion coefficient in most of the creeks. The key input parameters assigned are summarized in Table 5.

Table 5. Input parameters and simulated debris volume for pre-wildfire debris flows. Note that s and fs represent the solid phase and fine solid phase, respectively.

Creek	Internal Angle (s, fs)	Basal Friction (s, fs)	Erosion Coefficient	Generated Debris
Montecito	(25°, 10°)	(10°, 5°)	2.84×10^{-8}	34,000
San Ysidro	(25°, 10°)	(10°, 5°)	5.75×10^{-8}	41,000
Buena Vista	(25°, 10°)	(10°, 5°)	4.67×10^{-8}	5900
Romero	(25°, 10°)	(10°, 5°)	4.67×10^{-8}	15,200

As the volume of debris is reduced due to a higher basal friction and a reduced effective rainfall, the affected areas are also found to be smaller, except in Romero Creek. Accordingly, the simulated debris volume in Montecito Creek, San Ysidro Creek, Buena Vista Creek and Romero Creek is reduced by 85.0%, 85.9%, 85.5% and 84.7%, respectively. Overall, the debris flows affected by the wildfire across all creeks are substantially stronger and larger than in the pre-wildfire scenarios.

5. Concluding Remarks

Wildfires and post-wildfire hazards continue to pose a significant threat to communities around the world. A field survey of the Montecito wildfire shows that many areas around the catchment of the four major creeks in the study area were significantly burnt. These areas are also where the debris flows were concentrated that took place one month later. The rainfall data recorded at the weather stations nearby suggest that the intensive 1 h of rainfall could be the trigger that led to several debris flows around the major four creeks.

A multi-phase flow model is adopted in the present study to investigate the characteristics of the debris flows around Montecito, especially the post-wildfire conditions caused by the wildfires, which could possibly weaken the soil resistance to sliding or flowing while enhancing soil erosion. The simulated debris volumes around the four creeks are reasonably consistent with the estimations from earlier field observations, as the differences are around 1~7%. Overall, the areas affected by debris flows also agree fairly well with those that were observed in the field. A similar simulation of the pre-wildfire scenario indicates the debris would be much less significant before the wildfire. While understanding the complex behavior of debris flows remains a major challenge and the mechanisms of wildfires' effects on the soil or sediment behavior are yet to be fully explored, the present study demonstrates the potential of a quantitative approach to address the physical and mechanical processes involved in post-wildfire geological hazards.

Author Contributions: Conceptualization, D.K.C.; methodology, D.K.C. and L.H.; software, D.K.C. and M.W.N.; formal analysis, D.K.C.; investigation, D.K.C.; resources, L.H.; data curation, D.K.C.; writing—original draft preparation, D.K.C. and L.H.; writing—review and editing, L.H.; visualization, D.K.C. and M.W.N.; supervision, L.H.; project administration, L.H. All authors have read and agreed to the published version of the manuscript.

Funding: This research received no external funding.

Data Availability Statement: Data used in the present study is contained within the article.

Acknowledgments: The first author (D.K.C.) and third author (L.H.) wish to acknowledge the financial support provided by the University of Toledo through a Summer Research Fellowship during the preparation of this manuscript.

Conflicts of Interest: Author Diwakar K. C. was employed by the company Geotechnology LLC. The remaining authors declare that the research was conducted in the absence of any commercial or financial relationships that could be construed as a potential conflict of interest.

References

1. Flannigan, M.D.; Bergeron, Y.; Engelmark, O.; Wotton, B.M. Future wildfire in circumboreal forests in relation to global warming. *J. Veg. Sci.* **1998**, *9*, 469–476. [[CrossRef](#)]
2. Running, S.W. Is global warming causing more, larger wildfires? *Science* **2006**, *313*, 927–928. [[CrossRef](#)]
3. Sun, Q.; Miao, C.; Hanel, M.; Borthwick, A. G.; Duan, Q.; Ji, D.; Li, H. Global heat stress on health, wildfires, and agricultural crops under different levels of climate warming. *Environ. Int.* **2019**, *128*, 125–136. [[CrossRef](#)] [[PubMed](#)]
4. Shi, G.; Yan, H.; Zhang, W.; Dodson, J.; Heijnis, H.; Burrows, M. Rapid warming has resulted in more wildfires in northeastern Australia. *Sci. Total Environ.* **2021**, *771*, 144888. [[CrossRef](#)]
5. Santi, P.M.; dewolfe, V.G.; Higgins, J.D.; Cannon, S.H.; Gartner, J.E. Sources of debris flow material in burned areas. *Geomorphology* **2008**, *96*, 310–321. [[CrossRef](#)]
6. Cannon, S.H.; DeGraff, J. The increasing wildfire and post-fire debris-flow threat in western USA, and implications for consequences of climate change. In *Landslides-Disaster Risk Reduction*; Springer: Berlin/Heidelberg, Germany, 2009; pp. 177–190.
7. Ren, D.; Leslie, L.M. Climate warming enhancement of catastrophic southern California debris flows. *Sci. Rep.* **2020**, *10*, 10507. [[CrossRef](#)] [[PubMed](#)]
8. Campo, J.; Andreu, V.; Gimeno-Garcia, E.; Gonzalez, O.; Rubio, J. L. Occurrence of soil erosion after repeated experimental fires in a Mediterranean environment. *Geomorphology* **2006**, *82*, 376–387. [[CrossRef](#)]
9. Moody, J.A.; Kinner, D.A.; Ubeda, X. Linking hydraulic properties of fire-affected soils to infiltration and water repellency. *J. Hydrol.* **2009**, *379*, 291–303. [[CrossRef](#)]
10. Ebel, B.A.; Moody, J.A. Rethinking infiltration in wildfire-affected soils. *Hydrol. Processes* **2013**, *27*, 1510–1514. [[CrossRef](#)]
11. Meyer, G.A.; Wells, S.G.; Timothy Jull, A.J. Fire and alluvial chronology in Yellowstone National Park: Climatic and intrinsic controls on Holocene geomorphic processes. *Geol. Soc. Am. Bull.* **1995**, *107*, 1211–1230. [[CrossRef](#)]
12. Cannon, S.H.; Reneau, S.L. Conditions for generation of fire-related debris flows, Capulin Canyon, New Mexico. *Earth Surf. Processes Landforms* **2000**, *25*, 1103–1121. [[CrossRef](#)]
13. Kean, J.W.; Staley, D.M.; Cannon, S.H. In situ measurements of post-fire debris flows in southern California: Comparisons of the timing and magnitude of 24 debris? Flow events with rainfall and soil moisture conditions. *J. Geophys. Res. Earth Surf.* **2011**, *116*, F04019. [[CrossRef](#)]
14. Cannon, S.H.; Kirkham, R.M.; Parise, M. Wildfire-related debris-flow initiation processes, Storm King Mountain, Colorado. *Geomorphology* **2001**, *39*, 171–188. [[CrossRef](#)]
15. Nyman, P.; Sheridan, G.J.; Smith, H.G.; Lane, P.N. Evidence of debris flow occurrence after wildfire in upland catchments of south-east Australia. *Geomorphology* **2011**, *125*, 383–401. [[CrossRef](#)]
16. Bagnold, R.A. Experiments on a gravity-free dispersion of large solid spheres in a Newtonian fluid under shear. *Proc. R. Soc. Lond. Ser. A Math. Phys. Sci.* **1954**, *225*, 49–63.
17. Savage, S.B. Gravity flow of cohesionless granular materials in chutes and channels. *J. Fluid Mech.* **1979**, *92*, 53–96. [[CrossRef](#)]
18. Takahashi, T. Debris flow. *Annu. Rev. Fluid Mech.* **1981**, *13*, 57–77. [[CrossRef](#)]
19. DeLeon, A.A.; Jeppson, R.W. *Hydraulic and Numerical Solutions of Steady-State but Spatially Varied Debris Flow*; Utah Water Research Laboratory, Utah State University: Logan, UT, USA, 1982; pp. 4–24.
20. Takahashi, T.; Tsujimoto, H. Delineation of the debris flow hazardous zone by a numerical simulation method. In Proceedings of the International Symposium on Erosion, Debris Flow and Disaster Prevention, Tsukuba, Japan, 3–5 September 1985; pp. 457–462.
21. O'Brien, J.S. Physical Processes, Rheology and Modeling of Mudflows. Ph.D. Thesis, Colorado State University, Fort Collins, CO, USA, 1986.
22. Savage, S.B., Hutter, K. The motion of a finite mass of granular material down a rough incline. *J. Fluid Mech.* **1989**, *199*, 177–215. [[CrossRef](#)]
23. Ancey, C. Dry granular flows down an inclined channel: Experimental investigations on the frictional-collisional regime. *Phys. Rev.* **2001**, *65*, 011304. [[CrossRef](#)]
24. Midi, G.D.R. On dense granular flows. *Eur. Phys. J.* **2004**, *14*, 341–365.
25. Perez, S.; Aharonov, E.; Toussaint, R. Unsteady granular flows down an inclined plane. *Phys. Rev.* **2016**, *93*, 042902. [[CrossRef](#)] [[PubMed](#)]
26. Jop, P.; Forterre, Y.; Pouliquen, O. A constitutive law for dense granular flows. *Nature* **2006**, *441*, 727–730. [[CrossRef](#)] [[PubMed](#)]
27. Denlinger, R.P.; Iverson, R.M. Flow of variably fluidized granular masses across three dimensional terrain: 2. Numerical predictions and experimental tests. *J. Geophys. Res. Solid Earth* **2001**, *106*, 553–566. [[CrossRef](#)]
28. Pitman, E.B.; Le, L. A two-fluid model for avalanche and debris flows. *Philos. Trans. R. Soc. A* **2005**, *363*, 1573–1601. [[CrossRef](#)]

29. Hutter, K.; Schneider, L. Important aspects in the formulation of solid-fluid debris-flow models. Part I: Thermodynamic implications. In *Continuum Mechanics and Thermodynamics*; Springer: Berlin/Heidelberg, Germany, 2010; Volume 22, pp. 363–390.
30. Pudasaini, S.P. A general two-phase debris flow model. *J. Geophys. Res. Earth Surf.* **2012**, *117*, F03010. [CrossRef]
31. Luca, I.; Tai, Y.C.; Kuo, C.Y. *Shallow Geophysical Mass Flows Down Arbitrary Topography*; Springer: Berlin/Heidelberg, Germany, 2016; pp. 203–250.
32. Pudasaini, S.P.; Mergili, M. A multi-phase mass flow model. *J. Geophys. Res. Earth Surf.* **2019**, *124*, 2920–2942. [CrossRef]
33. Keller, E.; Adamaitis, C.; Alessio, P.; Goto, E.; Gray, S.; Heermance, R.V.; Schwartz, J.J. Montecito debris flows of 9 January 2018: Physical processes and social implications. In *From the Islands to the Mountains: A*; Geological Society of America: Boulder, CO, USA, 2020; pp. 95–114.
34. Kean, J.W.; Staley, D.M.; Lancaster, J.T.; Rengers, F.K.; Swanson, B.J.; Coe, J.A.; Hernandez, J.L.; Sigman, A.J.; Allstadt, K.E.; Lindsay, D.N. Inundation, flow dynamics, and damage in the 9 January 2018 Montecito debris-flow event, California, USA: Opportunities and challenges for post-wildfire risk assessment. *Geosphere* **2019**, *15*, 1140–1163. [CrossRef]
35. Flash Flood & Debris Flow Event Montecito, California January 9, 2018. Available online: <https://noaa.maps.arcgis.com/apps/MapJournal/index.html?appid=541c23aa483b48978d1bc9904a6fb14d> (accessed on 20 February 2022).
36. Ventura County Fire Department (VCFD). VCFD Determines Cause of the Thomas Fire. Available online: <https://vcfd.org/news/vcfดetermines-cause-of-the-thomas-fire> (accessed on 27 May 2022).
37. United States Geological Survey (USGS). Available online: <https://earthexplorer.usgs.gov/> (accessed on 1 March 2022).
38. Copernicus Open Access Hub. Available online: <https://scihub.copernicus.eu/> (accessed on 1 May 2022).
39. Meddens, A.J.; Kolden, C.A.; Lutz, J.A. Detecting unburned areas within wildfire perimeters using Landsat and ancillary data across the northwestern United States. *Remote Sens. Environ.* **2016**, *186*, 275–285. [CrossRef]
40. Hislop, S.; Jones, S.; Soto-Berelov, M.; Skidmore, A.; Haywood, A.; Nguyen, T.H. Using landsat spectral indices in time-series to assess wildfire disturbance and recovery. *Remote Sens.* **2018**, *10*, 460. [CrossRef]
41. KC, D.; Hu, L. Post-Wildfire Debris Flows in Montecito, California (USA): A Case Study and Empirically Based Debris Volume Estimation. *Geotechnics* **2023**, *3*, 347–359. [CrossRef]
42. Zoomash Ltd. WorldWeather Online (WWO). Available online: <https://www.worldweatheronline.com/> (accessed on 14 January 2022).
43. Cui, Y.; Cheng, D.; Chan, D. Investigation of post-fire debris flows in Montecito. *ISPRS Int. J. Geo Inf.* **2018**, *8*, 5. [CrossRef]
44. Alessio, P.; Dunne, T.; Morell, K. Post-wildfire generation of debris-flow slurry by rill erosion on colluvial hillslopes. *J. Geophys. Res. Earth Surf.* **2021**, *126*, e2021JF006108. [CrossRef]
45. Mergili, M.; Fischer, J.-T.; Krenn, J.; Pudasaini, S.P. ravaflow v1, an advanced open-source computational framework for the propagation and interaction of two-phase mass flows. *Geosci. Model Dev.* **2017**, *10*, 553–569. [CrossRef]
46. Mergili, M.; Jaboyedoff, M.; Pullarello, J.; Pudasaini, S.P. Back calculation of the 2017 piz cengalo-bondo landslide cascade with ravaflow: What we can do and what we can learn. *Nat. Hazards Earth Syst. Sci.* **2020**, *20*, 505–520. [CrossRef]
47. Naqvi, M.W.; KC, D.; Hu, L. Numerical modeling and a parametric study of various mass flows based on a multi-phase computational framework. *Geotechnics* **2022**, *2*, 506–522. [CrossRef]
48. Naqvi, M.W.; KC, D.; Hu, L. Numerical Modelling and Sensitivity Analysis of the Pitztal Valley Debris Flow Event. *Geosciences* **2023**, *13*, 378. [CrossRef]
49. Alaska Satellite Facility (ASF). Available online: <https://search.asf.alaska.edu> (accessed on 8 March 2022).
50. Baggio, T.; Mergili, M.; D’Agostino, V. Advances in the simulation of debris flow erosion: The case study of the Rio Gere (Italy) event of the 4th August 2017. *Geomorphology* **2021**, *381*, 107664. [CrossRef]
51. Stoof, C.R.; Ferreira, A.J.; Mol, W.; Van den Berg, J.; De Kort, A.; Drooger, S.; Slingerland, E.C.; Mansholt, A.U.; Ferreira, C.S.; Ritsema, C.J. Soil surface changes increase runoff and erosion risk after a low-moderate severity fire. *Geoderma* **2015**, *239*, 58–67. [CrossRef]

Disclaimer/Publisher’s Note: The statements, opinions and data contained in all publications are solely those of the individual author(s) and contributor(s) and not of MDPI and/or the editor(s). MDPI and/or the editor(s) disclaim responsibility for any injury to people or property resulting from any ideas, methods, instructions or products referred to in the content.